# Breakdown of the adiabatic Born–Oppenheimer approximation in graphene

SIMONE PISANA[1], MICHELE LAZZERI[2], CINZIA CASIRAGHI[1], KOSTYA S. NOVOSELOV[3], A. K. GEIM[3], ANDREA C. FERRARI[1]* AND FRANCESCO MAURI[2]*

[1]Engineering Department, Cambridge University, Cambridge CB3 0FA, UK
[2]IMPMC, Universités Paris 6 et 7, CNRS, IPGP, 140 rue de Lourmel, 75015 Paris, France
[3]Department of Physics and Astronomy, University of Manchester, Manchester M13 9PL, UK
*e-mail: acf26@eng.cam.ac.uk; francesco.mauri@impmc.jussieu.fr

Published online: 11 February 2007; doi:10.1038/nmat1846

**The adiabatic Born–Oppenheimer approximation (ABO) has been the standard ansatz to describe the interaction between electrons and nuclei since the early days of quantum mechanics[1,2]. ABO assumes that the lighter electrons adjust adiabatically to the motion of the heavier nuclei, remaining at any time in their instantaneous ground state. ABO is well justified when the energy gap between ground and excited electronic states is larger than the energy scale of the nuclear motion. In metals, the gap is zero and phenomena beyond ABO (such as phonon-mediated superconductivity or phonon-induced renormalization of the electronic properties) occur[3]. The use of ABO to describe lattice motion in metals is, therefore, questionable[4,5]. In spite of this, ABO has proved effective for the accurate determination of chemical reactions[6], molecular dynamics[7,8] and phonon frequencies[9–11] in a wide range of metallic systems. Here, we show that ABO fails in graphene. Graphene, recently discovered in the free state[12,13], is a zero-bandgap semiconductor[14] that becomes a metal if the Fermi energy is tuned applying a gate voltage[13,15], $V_g$. This induces a stiffening of the Raman G peak that cannot be described within ABO.**

Graphene samples are prepared by micromechanical cleavage of bulk graphite at the surface of an oxidized Si wafer with a 300-nm-thick oxide layer, following the procedures described in ref. 12. This allows us to obtain graphene monocrystals exceeding 30 μm in size, Fig. 1a. Using photolithography, we then make Au/Cr electrical contacts, which allow the application of a gate voltage, $V_g$, between the Si wafer and graphene (Fig. 1a,b). The resulting devices are characterized by electric-field-effect measurements[13,15,16], yielding a charge-carrier mobility, $\mu$, of 5,000–10,000 $cm^2 V^{-1} s^{-1}$ at 295 K and a zero-bias ($V_g = 0$) doping of $\sim 10^{12}$ $cm^{-2}$. This is reflected in the existence of a finite gate voltage, $V_n$, at which the Hall resistance is zero and the longitudinal resistivity reaches its maximum. Accordingly, a positive (negative) $V_g$–$V_n$ induces electron (hole) doping, having an excess-electron surface concentration of $n = \eta(V_g - V_n)$. The coefficient $\eta \approx 7.2 \times 10^{10}$ $cm^{-2} V^{-1}$ is found from Hall effect measurements and agrees with the geometry of the resulting capacitor[12,13,15].

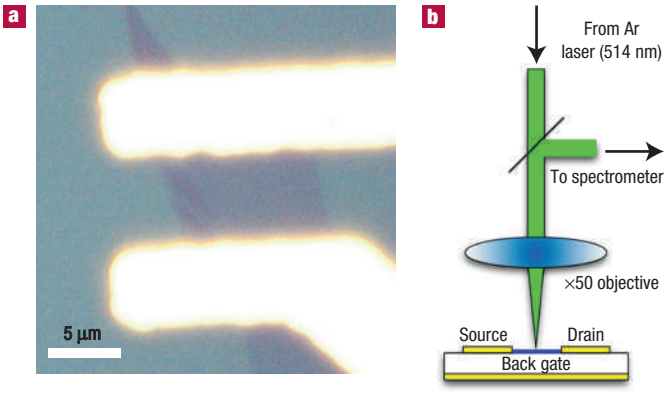


**Figure 1 Experimental set-up. a**, Optical micrograph of the contacted graphene sample. **b**, Schematic diagram of the Raman and transport set-up. The laser spot size is ~1 $\mu m^2$.

Unpolarized Raman spectra are measured at 295 and 200 K in ambient air and in vacuum ($<5 \times 10^{-6}$ mbar), respectively, with a Renishaw spectrometer at 514 nm using a ×50 long-working-distance objective, Fig. 1b. The incident power is kept well below 4 mW to avoid sample damage or laser-induced heating[17]. The Raman spectra are measured as a function of the applied $V_g$, Fig. 2a. Each spectrum is collected for 30 s. The applied gate voltage tends to move $V_n$, especially at room temperature. We thus determine the $V_g$ corresponding to the minimum G-peak position, and use this to estimate $V_n$. The G peak upshifts with positive applied $V_g$–$V_n$ at room temperature (Fig. 2a,b) and at 200 K (Fig. 2c). A similar trend, albeit over a smaller voltage range, is observed for negative $V_g$–$V_n$. This upshift for both electron and hole doping is qualitatively similar to that reported by Yan *et al.* for electrically doped graphene measured at 10 K (ref. 18).

The Raman G peak of graphene corresponds to the $E_{2g}$ phonon at the Brillouin zone centre, $\Gamma$, (refs 17,19). Phonon calculations for undoped graphene and graphite show the presence of a Kohn

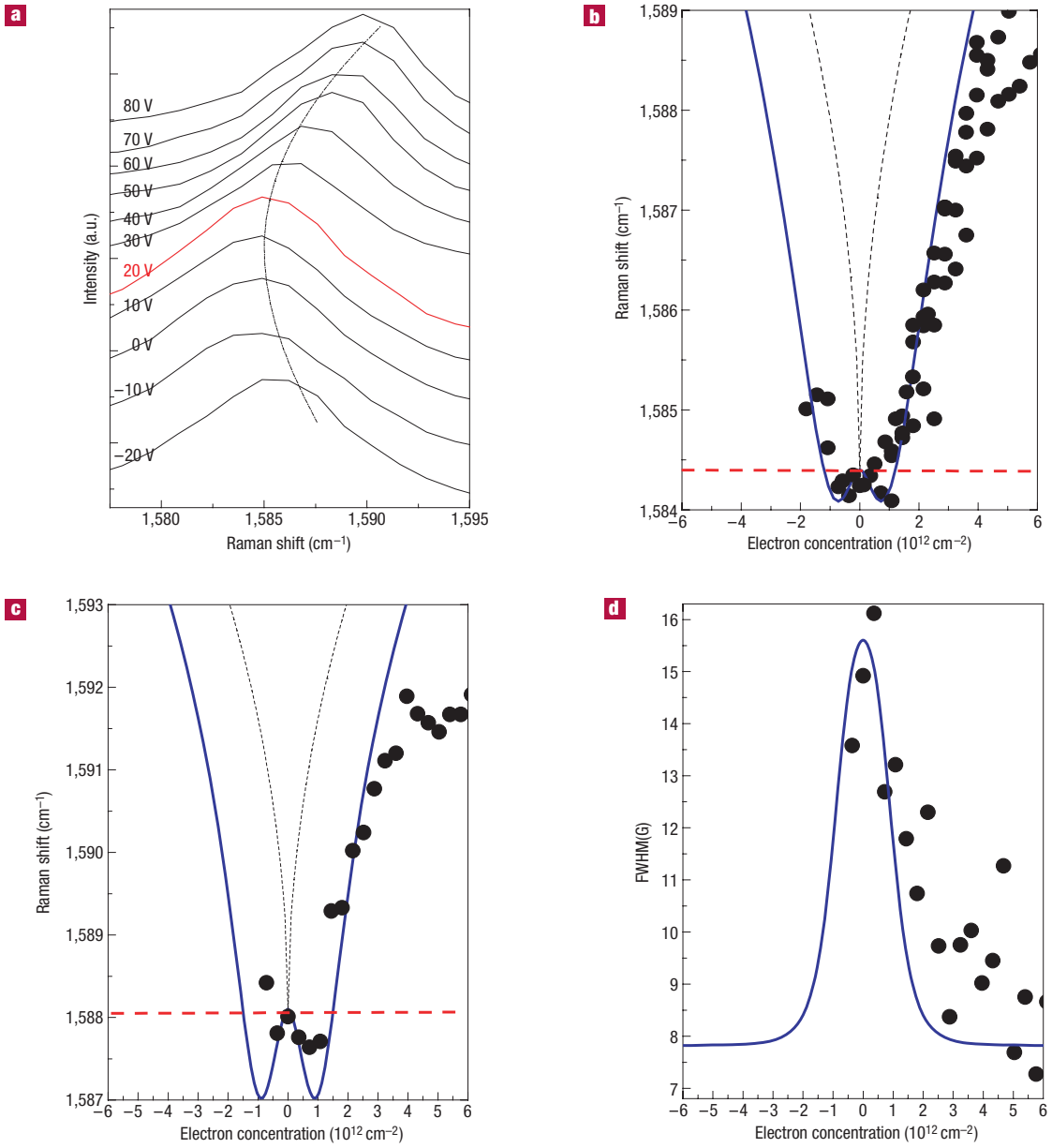


**Figure 2 Raman G peak of doped graphene. a**, Measurements at 295 K as a function of $V_g$. The red spectrum corresponds to the undoped case. **b**,**c**, G-peak position as a function of electron concentration at 295 K (**b**) and 200 K (**c**). Black circles: measurements; red dashed line: adiabatic Born–Oppenheimer; blue line: finite-temperature non-adiabatic calculation from equation (6); black dashed line: simplified non-adiabatic calculation from equation (5). The minimum observed in the calculations at $\sim 10^{12}$ cm$^{-2}$ occurs when the Fermi energy equals half of the phonon energy. **d**, FWHM(G) at 200 K as a function of electron concentration. Circles: measures; blue line: theoretical FWHM of a Voigt profile obtained from a lorentzian component given by equation (7) and a constant gaussian component of $\sim 8$ cm$^{-1}$.

anomaly in the phonon dispersion of the $E_{2g}$ mode near $\mathbf{\Gamma}$ (ref. 20). A Kohn anomaly is the softening of a phonon of wavevector $\mathbf{q} \sim 2\mathbf{k}_F$, where $\mathbf{k}_F$ is a Fermi-surface wavevector. By doping graphene, the change in the Fermi surface moves the Kohn anomaly away from $\mathbf{q} = \mathbf{0}$. Thus, as Raman spectroscopy probes phonons with $\mathbf{q} = \mathbf{0}$, intuitively we could expect a stiffening of the $\mathbf{q} = \mathbf{0}$ G peak. This would be in agreement with our experiments. To validate this picture, we need to compute the frequency of the $E_{2g}$ mode in doped graphene.

In graphene, the electronic bands near the high-symmetry **K** points are well described by a Dirac dispersion[14] $\epsilon(\mathbf{k}, \pi^*) = \hbar v_F k$ and $\epsilon(\mathbf{k}, \pi) = -\hbar v_F k$, where $\mathbf{k}+\mathbf{K}$ is the momentum of the Dirac Fermions, $v_F$ is the Fermi velocity and $\hbar v_F = 5.52$ eV Å, from density functional theory (DFT)[20] (Fig. 3a). The Dirac point is defined by the crossing of these conic bands and coincides with **K**, Fig. 3a. Thus, at zero temperature, the doping-induced shift of the Fermi level from the Dirac point is $\epsilon_F = \mathrm{sgn}(n)\sqrt{n\pi}\hbar v_F$, where $\mathrm{sgn}(x)$ is the sign of $x$.

The $E_{2g}$ phonon in graphene consists of an in-plane displacement of the carbon atoms by a vector $\pm\mathbf{u}/\sqrt{2}$ as shown in Fig. 3d. In the presence of such atomic displacements, the bands are still described by a cone (that is, a gap does not open) with the

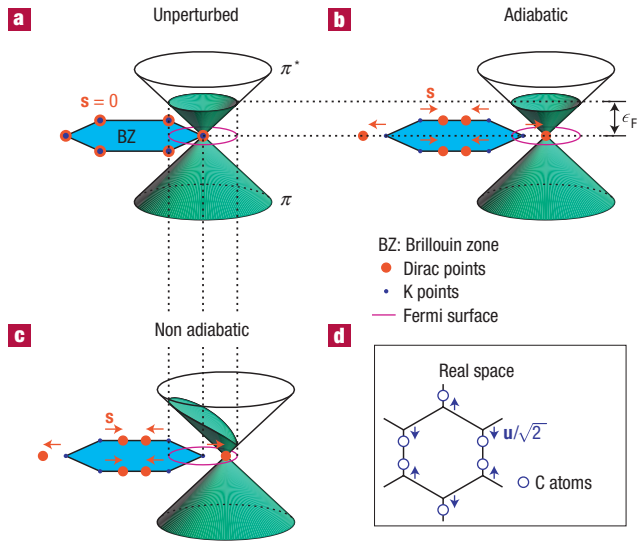


**Figure 3 Schematic $\pi$ band structure of doped graphene near the high-symmetry K point of the Brillouin zone.** The filled electronic states are shown in green. **a**, Bands of the perfect crystal. The Dirac point is at **K**, the electronic states are filled up to the Fermi energy $\epsilon_F$ and the Fermi surface is a circle centred at **K**. **b**, Bands in the presence of an $E_{2g}$ lattice distortion. The Dirac points are displaced from **K** by $\pm$**s**. Within ABO, the electrons remain in the instantaneous ground state: the bands are filled up to $\epsilon_F$ and the Fermi surface follows the Dirac-point displacement. The total electron energy does not depend on **s**. **c**, Bands in the presence of an $E_{2g}$ lattice distortion. In the non-adiabatic case, the electrons do not have time to relax their momenta (through impurity, electron–electron and electron–phonon scattering) to follow the instantaneous ground state. In the absence of scattering, the electron momentum is conserved and a state with momentum **k** is occupied if the state with the same **k** is occupied in the unperturbed case. As a consequence, the Fermi surface is the same as in the unperturbed case and does not follow the Dirac-cone displacement. The total electron energy increases with $s^2$, resulting in the observed $E_{2g}$-phonon stiffening. **d**, Atomic pattern of the $E_{2g}$ phonon. The atoms are displaced from the equilibrium positions by $\pm\mathbf{u}/\sqrt{2}$. Note that the displacement pattern of the Dirac points (in reciprocal space) is identical to the displacement pattern of the carbon atoms (in real space).

Dirac point shifted from **K** by a vector **s** (Fig. 3b,c)[21]. In practice, the atomic pattern of the $E_{2g}$ vibrations is mirrored into an identical pattern of Dirac-point vibrations in the reciprocal space. The dependence of the electronic bands on **u** can be obtained from the DFT electron–phonon coupling matrix elements (see equation (6) and note 24 of ref. 20 and Supplementary Information):

$$\epsilon(\mathbf{k}, \pi^*/\pi, \mathbf{u}) = \pm\hbar v_F|\mathbf{k} - \mathbf{s}(\mathbf{u})| \qquad (1)$$

where $\mathbf{s}\cdot\mathbf{u} = 0$, $s = u\sqrt{2\langle D_\Gamma^2\rangle_F}/(\hbar v_F)$ and $\langle D_\Gamma^2\rangle_F = 45.6\,\mathrm{eV}^2\,\mathrm{Å}^{-2}$ is the deformation potential of the $E_{2g}$ mode[22]. Equation (1) well reproduces the modification of the DFT band structure of graphene owing to a static displacement (frozen phonon) of the atoms according to the G phonon pattern.

The knowledge of the electronic bands (in the presence of a phonon) allows the determination of the phonon energy $\hbar\omega_{\epsilon_F}$ as a function of $\epsilon_F$. In particular,

$$\hbar\Delta\omega = \hbar\omega_{\epsilon_F} - \hbar\omega_0 = \frac{\hbar}{2M\omega_0}\frac{\mathrm{d}^2\Delta E}{(\mathrm{d}u)^2}, \qquad (2)$$

where $M$ is the carbon mass, $\omega_0$ is the frequency in the undoped case, $\Delta\omega \ll \omega_0$ and $\Delta E$ is the variation of the electronic energy with $\epsilon_F$.

Within ABO, $\Delta E(u)$ is computed assuming a static atomic displacement. Under this hypothesis, for any given displacement **u**, the electrons are supposed to be in the ground state, that is, the bands are filled up to $\epsilon_F$ (Fig. 3b). Thus, the adiabatic $\Delta E$ is

$$\Delta E(u) = \frac{4A}{(2\pi^2)}\int_{\epsilon(\mathbf{k},\pi^*,\mathbf{u})<\epsilon_F} \epsilon(\mathbf{k}, \pi^*, \mathbf{u})\,\mathrm{d}^2k, \qquad (3)$$

where we consider $\epsilon_F > 0$, $A = 5.24\,\mathrm{Å}^2$ is the unit-cell area and a factor of 4 accounts for spin and **K**-point degeneracy. Combining equations (1) and (3), we find that $\Delta E$ does not depend on **u** and $\hbar\Delta\omega = 0$. Thus, within ABO, the Raman G-peak position is independent of $\epsilon_F$, in contrast with experiments, Fig. 2b,c.

This failure of the frozen-phonon calculation urges us to re-examine the assumptions underlying ABO. The $E_{2g}$ phonon is a dynamical perturbation described by a time-dependent lattice displacement $\tilde{\mathbf{u}}(t) = \mathbf{u}\cos(\omega_0 t)$ oscillating at the G-peak frequency. Within ABO, it is assumed that, at any given time $t$, the electrons are in the adiabatic ground state of the instantaneous band structure $\epsilon(\mathbf{k}, \pi^*, \tilde{\mathbf{u}}(t))$. However, the inverse of the G-peak pulsation is $\sim$3 fs, which is much smaller than the typical electron-momentum relaxation times $\tau_m$ (owing to impurity, electron–electron and electron–phonon scattering with non-zero momentum phonons). Indeed, a $\tau_m$ of a few hundred femtoseconds is deduced from the electron mobility in graphene[23] and from ultrafast spectroscopy in graphite[24,25]. As a consequence, the electrons do not have time to relax their momenta to reach the instantaneous adiabatic ground state, as assumed in ABO. The departure from the adiabatic ground state can be accounted for in the calculation of $\Delta E$, by filling the perturbed bands, $\epsilon(\mathbf{k}, \pi^*, \mathbf{u})$ with the occupations of the unperturbed bands $\epsilon(\mathbf{k}, \pi^*, \mathbf{0})$, as in Fig. 3c:

$$\Delta E(u) = \frac{4A}{(2\pi^2)}\int_{\epsilon(\mathbf{k},\pi^*,\mathbf{0})<\epsilon_F} \epsilon(\mathbf{k}, \pi^*, \mathbf{u})\,\mathrm{d}^2k + \mathrm{O}(u^3). \qquad (4)$$

This equation is valid in the limit $\epsilon_F \gg \hbar\omega_0/2$, and can be rigorously derived using time-dependent perturbation theory, as shown in the Supplementary Information. In this case, the non-adiabatic energy, $\Delta E$, depends on $u$. Combining equations (1), (4) and (2) and carrying out the integral we get:

$$\hbar\Delta\omega = \frac{\hbar A\langle D_\Gamma^2\rangle_F}{\pi M\omega_0(\hbar v_F)^2}|\epsilon_F| = \alpha'|\epsilon_F|, \qquad (5)$$

where $\alpha' = 4.39\times10^{-3}$.

The result of equation (5) can be extended to any $\epsilon_F$ and finite temperature $T$ by computing the real part of the phonon self-energy[3] with the DFT electron–phonon coupling matrix elements (equation (6) and note 24 of ref. 20) to obtain:

$$\hbar\Delta\omega = \alpha' \mathrm{P}\int_{-\infty}^{\infty}\frac{[f(\epsilon-\epsilon_F) - f(\epsilon)]\epsilon^2\mathrm{sgn}(\epsilon)}{\epsilon^2 - (\hbar\omega_0)^2/4}\mathrm{d}\epsilon, \qquad (6)$$

where P is the principal part and $f$ is the Fermi–Dirac distribution at $T$ (refs 26–28). Figure 2b,c show the excellent agreement of our non-adiabatic finite $T$ calculation (equation (6)) with the experiments. The measured trends are also well captured by the simplified model, equation (5). By comparing the adiabatic and non-adiabatic calculations, we conclude that the stiffening of the $E_{2g}$ mode with $|\epsilon_F|$ is due to the departure of the electron population from the adiabatic ground state.

A pictorial interpretation of this phenomenon (valid for $\epsilon_F \gg \hbar\omega_0/2$) can be obtained by considering what happens to a filled glass when shaken horizontally. The liquid gravitational energy and its level mimic the electronic energy $\Delta E$ and $\epsilon_F$, respectively. The shaking frequency mimics the phonon frequency and the relaxation time of the liquid surface mimics the electron relaxation time. If the motion of the glass is slow, the liquid surface remains flat and its gravitational energy is independent of the glass horizontal position, as in equation (3) and in Fig. 3b. If the motion of the glass is rapid, the liquid surface profile is not flat and its gravitational energy increases with the displacement of the glass, as in equation (4) and Fig. 3c. To push the analogy even further, a non-cylindrical glass should be used, where the liquid surface increases with the liquid level. In this case, the higher the liquid level, the larger the difference between the gravitational energies in the fast- and slow-shaken glasses. Indeed, in graphene, the higher the Fermi level, the larger the difference between the non-adiabatic $\Delta E$ and the adiabatic $\Delta E$. This causes the observed stiffening of the phonon frequency with $\epsilon_F$.

The validity of our model is further confirmed by the analysis of the G-peak linewidth. The phonon decaying into an electron–hole pair gives the most important contribution to the homogeneous broadening of the $E_{2g}$ phonon. The full-width at half-maximum (FWHM), $\gamma$, can be computed extending to finite $T$ and $\epsilon_F \neq 0$ the results of ref. 22:

$$\gamma = \frac{\pi^2 \omega_0 \alpha'}{c}\left[f\left(-\frac{\hbar\omega_0}{2}-\epsilon_F\right)-f\left(\frac{\hbar\omega_0}{2}-\epsilon_F\right)\right], \qquad (7)$$

where $c$ is the speed of light. At $T = 0$, $\gamma = 11\,\mathrm{cm}^{-1}$ for $\epsilon_F = 0$ and $\gamma$ drops to zero for $\epsilon_F > \hbar\omega_0/2$ because the scattering process is forbidden by the Pauli exclusion principle[22]. Figure 2d shows a good agreement between the experimental and theoretical $\gamma$, once a constant inhomogeneous gaussian broadening of $\sim 8\,\mathrm{cm}^{-1}$ is added to the electron–phonon contribution of equation (7).

In summary, graphene is a remarkable example of ABO violation. Within ABO, the energy of a zone-centre phonon is determined by two contributions: the distortion of the electronic bands, associated with the phonon displacement, and the adiabatic rearrangement of the Fermi surface. In graphene, these two contributions cancel out exactly because of the peculiar rigid motion of the Dirac cones, associated with the $E_{2g}$ phonon. In general, a correct phonon treatment should not include the adiabatic rearrangement of the Fermi surface whenever the electron-momentum relaxation time is longer than the inverse of the phonon pulsation, as occurs in graphene and in several metals (see, for example, Table 1.3 of ref. 29). Note that the stronger the electron–phonon coupling with $\mathbf{q} = \mathbf{0}$ phonons, the larger the difference between ABO and non-ABO frequencies. However, the lattice dynamics is well described by ABO if the electron–phonon coupling with $\mathbf{q} \neq \mathbf{0}$ phonons is so strong that the electron-momentum relaxation is faster than the lattice motion. We anticipate that the ABO breakdown described here will affect the vibrational properties of carbon nanotubes[30] and phonon-mediated superconductors. Furthermore, the resulting variation of the Raman active peaks in graphene and nanotubes can allow determination of the effective doping by Raman spectroscopy, with important consequences for basic and applied research.

Received 29 November 2006; accepted 18 January 2007; published 11 February 2007.

## References


1. Born, M. & Oppenheimer, J. R. Zur quantentheorie der molekeln. *Ann. Phys.* **84**, 457–484 (1927).
2. Ziman, J. M. *Electrons and Phonons* (Oxford Univ. Press, Oxford, 1960).
3. Grimvall, G. *The Electron-Phonon Interaction in Metals* (North-Holland, Amsterdam, 1981).
4. Ponosov, Y. S., Bolotin, G. A., Thomsen, C. & Cardona, M. Raman scattering in Os: Nonadiabatic renormalization of the optical phonon self energies. *Phys. Status Solidi B* **208**, 257–269 (1988).
5. White, J. D., Chen, J., Matsiev, D., Auerbach, D. J. & Wodtke, A. M. Conversion of large-amplitude vibration to electron excitation at a metal surface. *Nature* **433**, 503–505 (2005).
6. Kroes, G. J., Gross, A., Baerends, E. J., Scheffler, M. & McCormack, D. A. Quantum theory of dissociative chemisorption on metal surfaces. *Acc. Chem. Res.* **35**, 193–200 (2002).
7. Alfe, D., Gillan, M. J. & Price, G. D. The melting curve of iron at the pressures of the Earth's core from *ab initio* calculations. *Nature* **401**, 462–464 (1999).
8. Walker, B. G., Molteni, C. & Marzari, N. Ab initio molecular dynamics of metal surfaces. *J. Phys. Condens. Matter* **16**, S2575–S2596 (2004).
9. Chester, G. V. The theory of interaction of electrons with lattice vibrations in metals. *Adv. Phys.* **10**, 357–400 (1961).
10. Baroni, S., De Gironcoli, S., Dal Corso, A. & Giannozzi, P. Phonons and related crystal properties from density functional perturbation theory. *Rev. Mod. Phys.* **73**, 515–562 (2001).
11. Savrasov, S. Y. & Savrasov, D. Y. Electron-phonon interactions and related physical properties of metals from linear-response theory. *Phys. Rev. B* **54**, 16487–16501 (1996).
12. Novoselov, K. S. *et al.* Two dimensional atomic crystals. *Proc. Natl Acad. Sci. USA* **102**, 10451–10453 (2005).
13. Novoselov, K. S. *et al.* Electric field effect in atomically thin carbon films. *Science* **306**, 666–669 (2004).
14. Wallace, P. R. The band theory of graphite. *Phys. Rev.* **71**, 622–634 (1947).
15. Novoselov, K. S. *et al.* Two dimensional gas of massless Dirac fermions in graphene. *Nature* **438**, 197–200 (2005).
16. Zhang, Y., Tan, Y. W., Stormer, H. L. & Kim, P. Experimental observation of the quantum Hall effect and Berry's phase in graphene. *Nature* **438**, 201–204 (2005).
17. Ferrari, A. C. *et al.* Raman spectrum of graphene and graphene layers. *Phys. Rev. Lett.* **97**, 187401 (2006).
18. Yan, J., Zhang, Y., Kim, P. & Pinczuk, A. Electric field effect tuning of electron-phonon coupling in graphene. Preprint at <http://www.arxiv.org/cond-mat/0612634> (2006).
19. Tuinstra, F. & Koenig, J. Raman spectrum of graphite. *J. Chem. Phys.* **53**, 1126–1130 (1970).
20. Piscanec, S., Lazzeri, M., Mauri, F., Ferrari, A. C. & Robertson, J. Kohn anomalies and electron phonon interactions in graphite. *Phys. Rev. Lett.* **93**, 185503 (2004).
21. Dubay, O. & Kresse, G. Accurate density functional calculations for the phonon dispersion relations of graphite layer and carbon nanotubes. *Phys. Rev. B* **67**, 035401 (2003).
22. Lazzeri, M., Piscanec, S., Mauri, F., Ferrari, A. C. & Robertson, J. Phonon linewidths and electron-phonon coupling in graphite and nanotubes. *Phys. Rev. B* **73**, 155426 (2006).
23. Zhang, Y. *et al.* Landau-level splitting in graphene in high magnetic fields. *Phys. Rev. Lett.* **96**, 136806 (2006).
24. Moos, G., Gahl, C., Fasel, R., Wolf, M. & Hertel, T. Anisotropy of quasiparticle lifetimes and the role of disorder in graphite from ultrafast time-resolved photoemission spectroscopy. *Phys. Rev. Lett.* **87**, 267402 (2001).
25. Kampfrath, T., Perfetti, L., Schapper, F., Frischkorn, C. & Wolf, M. Strongly coupled optical phonons in the ultrafast dynamics of electronic energy and current relaxation in graphite. *Phys. Rev. Lett.* **95**, 187403 (2005).
26. Lazzeri, M. & Mauri, F. Non-adiabatic Kohn-anomaly in a doped graphene monolayer. *Phys. Rev. Lett.* **97**, 266407 (2006).
27. Ando, T. Anomaly of optical phonon in monolayer graphene. *J. Phys. Soc. Jpn.* **75**, 124701 (2006).
28. Castro Neto, A. H. & Guinea, F. Electron-phonon coupling and Raman spectroscopy in graphene. *Phys. Rev. B* **75**, 045404 (2007).
29. Ashcroft, N. W. & Mermin, N. D. *Solid State Physics* (Saunders College, London, 1976).
30. Piscanec, S., Lazzeri, M., Robertson, J., Ferrari, A. C. & Mauri, F. Optical phonons in carbon nanotubes: Kohn anomalies, peierls distortions and dynamic effects. *Phys. Rev. B* **75**, 035427 (2007).


## Acknowledgements

The authors thank P. Kim and A. Pinczuk for useful discussions and for sending us a preprint of ref. 18. A.C.F. acknowledges funding from the Royal Society and The Leverhulme Trust. The calculations were carried out at IDRIS (Orsay).
Correspondence and requests for materials should be addressed to A.C.F or F.M.
Supplementary Information accompanies this paper on www.nature.com/naturematerials.

## Competing financial interests

The authors declare that they have no competing financial interests.